Synthesis of robust tunable oscillators using mitogen activated protein kinase cascades

Systems and Synthetic Biology

ISSN 1872-5325
Volume 4
Number 4

Syst Synth Biol (2010)
4:331-341
DOI 10.1007/
s11693-011-9078-3

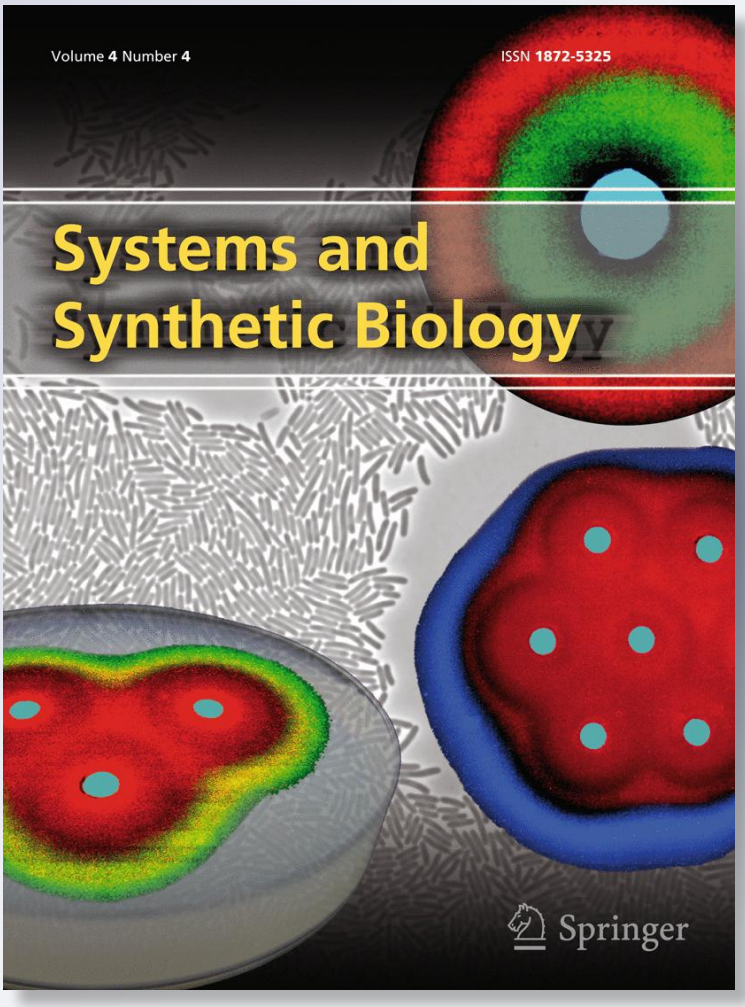

Springer

Syst Synth Biol (2010) 4:331–341
DOI 10.1007/s11693-011-9078-3

RESEARCH PAPER

Synthesis of robust tunable oscillators using mitogen activated protein kinase cascades

Vishwesh V. Kulkarni · Aditya Paranjape · Khem Raj Ghusinga · Naira Hovakimyan

Received: 13 December 2010 / Revised: 19 January 2011 / Accepted: 4 February 2011 / Published online: 6 March 2011

Abstract *Mitogen activated protein kinase* (MAPK) cascade is evolutionally preserved in all eukaryotic cells, and regulates various cellular activities such as gene expression, mitosis, differentiation, and apoptosis. Recently, Bashor et al. have shown that Ste5 scaffold protein can be used to reshape the MAPK cascade through engineered feedback loops, and have used heuristic tuning mechanisms to synthesize the feedback. A problem of interest is to determine whether information regarding the underlying biochemical reactions can be used to synthesize robust feedback that will ensure that the resultant circuit has the desired properties. In this paper, we consider the problem of engineering feedback in MAPK cascade to synthesize an oscillator of the desired frequency. Our approach builds on the MAPK cascade model derived by Chikarmane et al. who have exploited the existence of a Hopf bifurcation point in the Markevich model of the MAPK cascade to synthesize the exciting kinase as a function of the doubly phosphorylated protein. We show how the $\mathcal{L}_1$-control theory can be used for a robust synthesis of the oscillator and present the simulation results.

V. V. Kulkarni (✉) · K. R. Ghusinga
Department of Electrical Engineering, Indian Institute of Technology Bombay, Mumbai 400 076, India
e-mail: vishwesh@ee.iitb.ac.in

K. R. Ghusinga
e-mail: khemrajghusinga@gmail.com

A. Paranjape
Department of Aerospace Engineering, University of Illinois at Urbana-Champaign, Urbana, IL, USA
e-mail: aditya.paranjape@gmail.com

N. Hovakimyan
Department of Mechanical Science and Engineering, University of Illinois at Urbana-Champaign, Urbana, IL, USA
e-mail: nhovakim@illinois.edu

Keywords MAPK cascade · Oscillator · Nonlinearity · $\mathcal{L}_1$ controller

Introduction

Mitogen activated protein kinases (MAPK) are serine/threonine-specific protein kinases that respond to extracellular stimuli, viz. mitogens, and regulate various cellular activities such as gene expression, mitosis, differentiation, and apoptosis. Extracellular stimuli lead to activation of a MAPK via a signaling cascade, known as the MAPK cascade, comprising MAP kinase, *MAP kinase kinase* (MAP2K), and *MAP kinase kinase kinase* (MAP3K). An activated MAP3K phosphorylates a MAP2K on its serine and threonine residues. An activated MAP2K, in turn, phosphorylates a MAPK on its serine and threonine residues. The MAPK cascade is evolutionally preserved in all eukaryotic cells, ranging from yeasts to mammals (see Qiao et al. 2007). The MAPK cascade has been implicated in malignant transformations, and in the regulation of cellular growth and proliferation of several tumor types. For example, the active phosphorylated form of MAPK/ERK is aberrantly expressed in the cultured and primary Hodgkin disease cells (see Zheng et al. 2003). Therefore, mechanisms that can reshape the MAPK pathways signaling dynamics are of interest.

Recently, a platform based on the Ste5 scaffold protein has been developed to implement feedback in the MAPK cascade in order to alter its response to the mating pheromone stimulation (see Bashor et al. 2008). Several mathematical models, such as the Huang-Ferrell model (1996) and the Markevich model (2004), are known to characterize the biochemical reactions in the MAPK cascade reasonably well. Therefore, it should be possible to use

well-known system theoretic techniques to synthesize the required feedback controller, if it exists. For example, Chikarmane et al. have engineered a relay relaxation oscillator using the MAPK cascade by exploiting the fact that the Markevich model of the MAPK cascade exhibits a Hopf bifurcation point if a first order low pass filter is used as the feedback controller to synthesize the exciting kinase as a function of the doubly phosphorylated protein (see Chikarmane et al. 2007). In this paper, we use the well-known $\mathcal{L}_1$-control theory to characterize a class of feedback controllers to synthesize the exciting kinase as a function of the doubly phosphorylated protein so that the cascade now exhibits robust tunable oscillations in its output, i.e., in the doubly phosphorylated protein.

An advantage of the $\mathcal{L}_1$-control theory approach is that it enables one to decouple the problem of meeting the performance specifications and the problem of ensuring robustness to parameter variations and disturbances: the performance can be improved systematically by increasing the adaptation gain whereas the robustness is guaranteed—so long as it is feasible—by choosing an appropriate filter. Unlike the traditional adaptive control methodologies, the maximum adaptation gain is restricted only by limitations of the components used to implement the $\mathcal{L}_1$ controller. This ability to decouple the two problems is useful since a MAPK cascade is subject to parameter variations and disturbances (see Chikarmane et al. 2007; Qiao et al. 2007; Bashor et al. 2008).

The paper is organized as follows. In "Description of the MAPK cascade", we present the deterministic mathematical model of the MAPK cascade derived by Chikarmane et al. in 2007 and state the problem of interest. Since hysteresis has been shown to be a key property of the MAPK cascade, we present in "Background results" some background results on how oscillations can be induced in a hysteretic system by using an integrator or a low-pass-filter as the negative feedback. In Background on $\mathcal{L}_1$ adaptive controllers, we present an abridged introduction to $\mathcal{L}_1$ adaptive control. In "Synthesis of the $\mathcal{L}_1$ adaptive controller for the MAPK cascade", we synthesize an $\mathcal{L}_1$ adaptive controller that induces oscillations of the desired frequency in the MAPK cascade described in "Description of the MAPK cascade". In "Simulation results", we present the simulation results. In "Discussion", we briefly discuss how the control of MAPK cascade oscillations is important in cellular response and in the formation of hippocampal neuron memory. We conclude the paper in "Conclusion".

Description of the MAPK cascade

Modular structure of the MAPK cascade is shown in Fig. 1a. The symbols X, X_p, and X_{pp} represent, respectively, the unphosphorylated, single phosphorylated and doubly phosphorylated forms of the protein X. Each layer designates a distinct protein species: the first layer, populated with protein species M, is only singly phosphorylated whereas the two lower layers, populated by species N and O, are doubly phosphorylated. In each layer, forward reactions are catalysed by kinases and reverse reactions by phosphatases. Each forward reaction consumes ATP and releases ADP whereas and each reverse reaction releases the free phosphate (see Fig. 1b). In the lower two layers, the function performed by the kinase in the first layer is performed by the phosphorylated forms produced by the preceding layer. We now briefly summarize a dynamical model of the MAPK cascade as described in Chikarmane et al. (2007). In Chikarmane et al. (2007), the model derived by Markevich et al. (2004) is used to describe a kinetic scheme for the MAPK cascade wherein a two-site covalent modification cycle of a substrate M is acted upon by a phosphatase and a kinase, resulting in bistability of the cascade stage (see Markevich et al. 2004); experimental evidence for the bistability is presented in Wang et al. (2006) and Qiao et al. (2007). Figure 1b shows the reaction schemes of dual-phosphorylation subnetwork with three

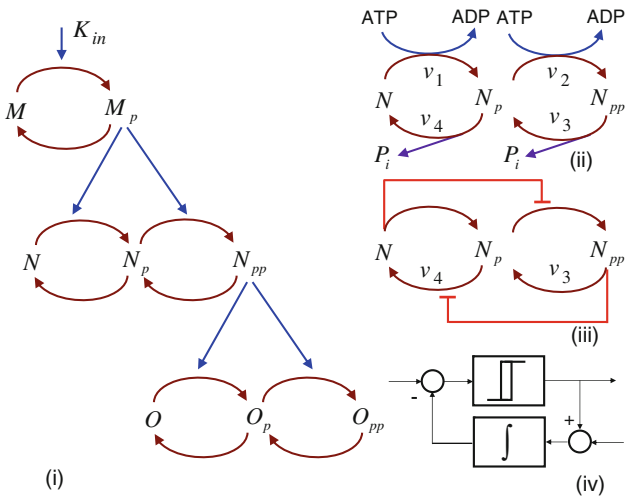

Fig. 1 **a** Hierarchical 3-tier structure of a typical MAPK signaling cascade (see Chikarmane et al. 2007) with each tier designating different protein species. The symbols X, X_p, and X_{pp} represent the unphosphorylated, phosphorylated, and doubly phosphorylated forms of the protein X. **b** The dual phosphorylation scheme for the multisite phosphorylation—the forward reactions are the phosphorylation reactions and are catalysed by kinases whereas the reverse reactions are dephosphorylation reactions and are catalysed by phosphatases (see Chikarmane et al. 2007). **c** Implied regulation in the dual phosphorylation scheme due to the sequestration effects—N suppresses the phosphorylation of N_p whereas N_{pp} suppresses the dephosphorylation of N_p (see Chikarmane et al. 2007). **d** The MAPK cascade is known to exhibit hysteresis. It is shown in Varigonda and Georgiou (2001) that oscillations can be induced in a hysteretic system by using an integrator in its negative feedback path

states of increasing phosphorylation: N, N_p, and N_{pp}. A two-site covalent-modification cycle, of a substrate N, is acted upon by a phosphatase ($Phos$) and a kinase (K_{in}), both in a non-processive, distributive way, such that the activity of M, showed bistability. Figure 1b shows the reaction scheme of a dual phosphorylation subnetwork, with three states of increasing phosphorylation, N, N_p, and N_{pp}. All the arrows in Fig. 1b represent the reactions governed by the Michaelis Menten kinetics. The phosphorylation steps are assumed to be irreversible while the dephosphorylation steps are assumed to be irreversible and product sensitive. This scheme results in the sequestration of $Phos$, by its products, viz., N_p and N. The sequestration of modifying enzymes effectively adds inhibitory loops into the network (see Fig. 1c). The first inhibition occurs when M suppresses the dephosphorylation of N_p. The second inhibition occurs when N_{pp} suppresses the dephosphorylation of M_p which occurs because N_{pp} sequesters Phos, thereby reducing its availability to N_p. These interactions lead to a positive feedback loop that stimulates the production of N_{pp}. The physical explanation for this is as follows. Increasing the kinase activity on v_1 and v_2 (see Fig. 1c) results in additional production of N_{pp}. The additional N_{pp} sequesters phosphatase which means that N_p is not consumed as fast and tends to rise. By conservation this must result in a decline in N. The increase in N_p stimulates further increases in N_{pp} which thereby creates the positive feedback. The increase in N_{pp} is further ensured by making sure that the N_{pp} phosphatase is near saturation, thus preventing the additional N_{pp} being dissipated by dephosphorylation. In addition, the rise in N_p is also enhanced by making sure that the kinase v_1, with respect to N, is close to saturation. These factors together result in bistability. Let $x \doteq [N\, N_p\, N_{pp}]^T$ and let $N_t \doteq N + N_p + N_{pp}$. Then, the MAPK cascade is described as follows (see Chikarmane et al. 2007):

$$\frac{dx}{dt} = \begin{bmatrix} v_4 - v_1 \\ -((v_4 - v_1) - (v_2 - v_3)) \\ v_2 - v_3 \end{bmatrix},$$

where

$$v_1 = \frac{k_1(K_{in}/K_{m1})N}{1 + N_P/K_{m_2} + N/K_{m1}},$$

$$v_2 = \frac{k_2(K_{in}/K_{m2})N_P}{1 + N_P/K_{m_2} + N/K_{m1}},$$

$$v_3 = \frac{k_3(Phos/K_{m3})N_{PP}}{1 + N_{PP}/K_{m3} + N_P/K_{m4} + N/K_{m5}},$$

$$v_4 = \frac{k_4(Phos/K_{m4})N_{PP}}{1 + N_{PP}/K_{m3} + N_P/K_{m4} + N/K_{m5}},$$

where the kinetic constants are as follows:

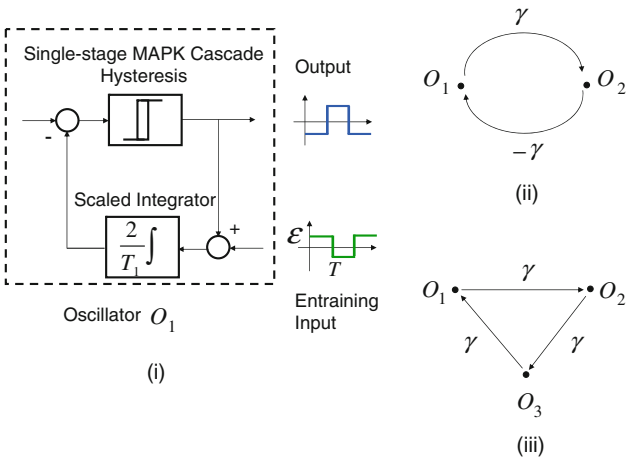

Fig. 2 **a** A relevant oscillator that entrains a given periodic input signal. It is shown in Varigonda and Georgiou (2001) that the region of entrainment increases with the increase in the magnitude of the input signal. The results of Varigonda and Georgiou (2001) can be used to induce oscillations in the motifs shown in **b** and **c**

$\kappa_1 = 0.01$, $\kappa_2 = 15$, $\kappa_3 = 0.06$, $\kappa_4 = 0.084$, $K_{m1} = 50$, $K_{m2} = 500$, $K_{m3} = 22$, $K_{m4} = 18$, $K_{m5} = 86$, $Phos = 100$, $N_t = 500$.

Let us refer to this system as $\mathcal{S}_1$. Setting $\dot{N} = \dot{N}_p = \dot{N}_{pp} = 0$, the necessary and sufficient condition for bistability in a single stage of the MAPK cascade are obtained. It is shown in Chikarmane et al. (2007) that the doubly phosphorylated protein output of a stage evolves as a hysteretic function of the exciting kinase, which is the exogenous input to this stage.

We are interested in synthesizing feedback mechanisms that will ensure oscillations in various network motifs featuring a MAPK cascade (see Fig. 2a–c). The motifs are of the following form: (1) a single stage of the MAPK cascade, (2) two interconnected single stages, and (3) a mesh network featuring three interconnected single stages.

Background results

Recent experimental results of Qiao et al. (2007) show that a majority of oscillations in the MAPK cascade are built around the single stage hysteresis. Indeed, it is well known in system theory that an oscillator can be obtained by wrapping an integrator feedback around a hysteretic element (see Varigonda and Georgiou 2001; Stan and Sepulchre 2007). The three network motifs for which the framework of Varigonda and Georgiou (2001) is directly applicable are shown in Fig. 2a–c. Figure 2a illustrates the structure of an oscillator O_i with the frequency of oscillation $1/2T_i$ ($i = 1, 2, 3$); the exciting input for this oscillator is a square wave of amplitude ε and frequency $1/2T$. Using

Theorems 1 and 2 of Varigonda and Georgiou (2001), the following results are established for the three motifs shown in Fig. 2.

Lemma 1 *Consider the single stage MAPK cascade motif shown in Fig. 2a. Define* $\sigma = T_1/T$. *Then, the entrainment by the forcing square wave of amplitude* ε *and frequency* $1/2T$ *is possible if* $\sigma \in [1-\varepsilon, 1+\varepsilon)$.

Lemma 2 *Consider the MAPK cascade motif shown in Fig. 2b. The oscillators* O_i *have the same structure as the oscillator shown in Fig. 2a but with frequencies* $1/2T_i$ $(i = 1, 2)$. *The oscillators are connected to each other through constant gains of* γ *and* $-\gamma$, *respectively, where* $\gamma > 0$. *Suppose* $T_2 \geq T_1$. *Then, the network motif oscillates in synchrony with* (i) O_2 *leading* O_1 *if* $\gamma > (T_2 - T_1)/(T_2 + T_1)$, *and* (ii) O_1 *leading* O_2 *if* $-\gamma > (T_2 - T_1)/(T_2 + T_1)$; *the mean half-period in both cases is* $(T_1 + T_2)/2$.

Similar results can be established for the network motif shown in Fig. 2c.

Remark 1 The motifs shown in Fig. 2 can be implemented in the Ste5 protein scaffold presented in Bashor et al. (2008) by varying the strength of the feedback signal at the recruited negative modulator site of the scaffold.

Remark 2 It is shown in Georgiou and Smith (2000) that O_1 is robust to changes in the linear time-invariant feedback if the scaled integrator is replaced by a time-delay linear time-invariant system, provided some additional constraints are satisfied. This modification is useful since the MAPK cascade is subject to exogenous disturbances (see Bashor et al. 2008; Hasty et al. 2001; Kholodenko et al. 2002).

Table 1 Notation

Symbol	Meaning
$(\cdot)^T$	Transpose of a vector or a matrix $(\cdot)$
$x, y\rangle$	$= \int_{-\infty}^{\infty} y^T(t)x(t)dt$ (inner product of x and y)
$\langle x, y\rangle_\ell$	$= \int_0^\ell y^T(t)x(t)dt$ (truncated inner product of x and y)
$\|x\|$	$= \sqrt{\langle x, x\rangle}$ (Euclidean norm of x)
$\|x\|_\ell$	$= \sqrt{\langle x, x\rangle_\ell}$ (Truncated norm of x)
$\|x\|_{\mathcal{L}_1}$ (or $\|x\|_{\mathcal{L}_\infty}$)	$\mathcal{L}_1$-norm (or $\mathcal{L}_\infty$-norm) of x
$\|x_t\|_{\mathcal{L}_1}$ or $(\|x_t\|_{\mathcal{L}_\infty})$	Truncated $\mathcal{L}_1$-norm or ($\mathcal{L}_\infty$-norm) of x
$\dot{x}$	First time-derivative of the signal x
$\ddot{x}$	Second time-derivative of the signal x
$\mathcal{L}(f)$	Laplace transform of the function f
Proj(x, y)	Projection operator
∇	Gradient operator
LTI (LTV)	Linear time-invariant (linear time-varying)

Background on $\mathcal{L}_1$ adaptive controllers

Definition 1 The $\mathcal{L}_1$ norm of a *bounded-input bounded-output* (BIBO) stable proper *single-input single-output* (SISO) LTI system is defined by

$$\|H(s)\|_{\mathcal{L}_1} = \int_0^\infty |h(t)|dt$$

where $h(t)$ is the impulse response of $H(s)$, computed via the inverse Laplace transform:

$$h(t) = \frac{1}{2\pi j}\int_{\alpha-j\infty}^{\alpha+j\infty} H(s)e^{st}ds, \quad t \geq 0,$$

in which the integration is taken along the vertical line with X-intercept at $\alpha > 0$ in the complex plane.

Proposition 1 *A continuous-time LTI proper system with impulse response* $h(t)$ *is stable if and only if its* $\mathcal{L}_1$ *gain is finite, i.e., if and only if* $\int_0^\infty |h(\tau)|\, d\tau < \infty$.

Remark 3 The above proposition is proved in Theorem 3.3.2, p. 81 (Ioannou and Sun 1996).

Definition 2 The $\mathcal{L}_1$ norm of a bounded-input bounded-output (BIBO) stable proper single-input single-output (SISO) linear-time-varying (LTV) system is defined by

$$\|H\|_{\mathcal{L}_1} = \sup_{\forall t, \tau \geq 0} \int_\tau^t |g(\sigma, t)|d\sigma$$

where $g(t, \sigma)$ is the impulse response of SISO system H.

Definition 3 The $\mathcal{L}_1$ gain of a BIBO stable proper m-input n-output (MIMO) LTI system $H(s)$ is defined as

$$\|H(s)\|_{\mathcal{L}_1} = \max_{i=1,\ldots,n}\left(\sum_{j=1}^m \|H_{ij}(s)\|_{\mathcal{L}_1}\right),$$

where $H_{ij}(s)$ is the ith row jth column element of $H(s)$.

Definition 4 The $\mathcal{L}_1$ norm of a BIBO stable proper MIMO LTV system is defined by

$$\|H\|_{\mathcal{L}_1} = \max_{i=1,\ldots,n}\left(\sum_{j=1}^m \|H_{ij}\|_{\mathcal{L}_1}\right)$$

where $\|H_{ij}\|_{\mathcal{L}_1} = \sup_{\forall t,\, \tau,\, t \geq \tau} \int_\tau^t |g_{ij}(t, \sigma)|d\sigma$.

Lemma 3 *For a stable proper MIMO LTI system with input* $r(t) \in \mathbb{R}^m$ *and output* $x(t) \in \mathbb{R}^n$, *we have* $\|x_t\|_{\mathcal{L}_\infty} \leq \|H\|_{\mathcal{L}_1}\|r_t\|_{\mathcal{L}_\infty}, \quad \forall t > 0.$

Remark 4 This lemma is an extension of the result in Example 5.2, p. 199 (Khalil 2002) to general MIMO systems.

Corollary 1 *For a stable proper MIMO LTI system $H(s)$, if the input $r(t) \in \mathbb{R}^m$ is bounded, then the output is also bounded as follows: $\|x\|_{\mathcal{L}_\infty} \leq \|H(s)\|_{\mathcal{L}_1} \|r\|_{\mathcal{L}_\infty}$.*

Lemma 4 *For a cascaded system $H(s) = H_2(s)H_1(s)$, where $H_1(s)$ is stable proper system with m inputs and l outputs and while $H_2(s)$ is a stable proper system with l inputs and n outputs, we have $\|H(s)\|_{\mathcal{L}_1} \leq \|H_2(s)\|_{\mathcal{L}_1} \|H_1(s)\|_{\mathcal{L}_1}$.*

Theorem 1 [$\mathcal{L}_1$ Small Gain Theorem] *The interconnection shown in the Fig. 3 is stable if $\|M(s)\|_{\mathcal{L}_1} \|\Delta(s)\|_{\mathcal{L}_1} < 1$.*

We next define the projection operator and state its relevant properties.

Definition 5 Consider a convex, compact set defined by $\Omega_c \doteq \{\boldsymbol{\theta} \in \mathbb{R}^n | f(\boldsymbol{\theta}) \leq c\}, \quad 0 \leq c \leq 1$, where $f : \mathbb{R}^n \to \mathbb{R}^n$ is the following smooth convex function:

$$f(\boldsymbol{\theta}) = \frac{\boldsymbol{\theta}^\top \boldsymbol{\theta} - \theta_{\max}^2}{\epsilon_\theta \theta_{\max}^2}$$

where $\theta_{\max}$ is the norm bound of the parameter vector $\boldsymbol{\theta}$ and ε_θ is the convergence tolerance. Let $\boldsymbol{\theta}^*$, the true value

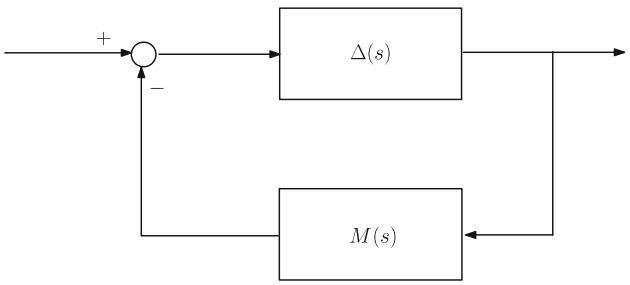

Fig. 3 The interconnected system examined in Theorem 1 (see Cao and Hovakimyan 2006). It is often of interest to decompose a given network as an interconnection of an easily analyzable subsystem $M(s)$, which is often a linear time-invariant system, and a more complex subsystem $\Delta(s)$

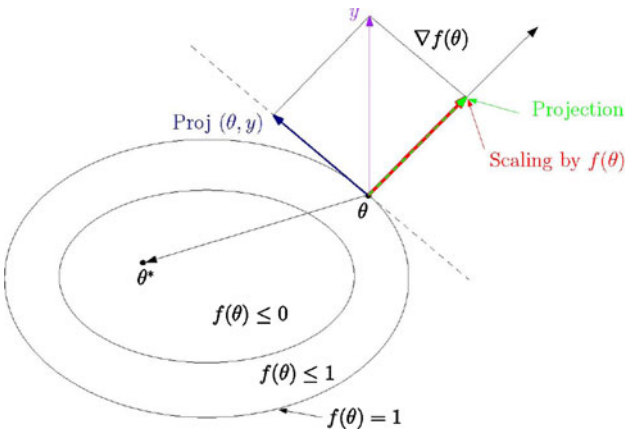

Fig. 4 An illustration of the projection operator

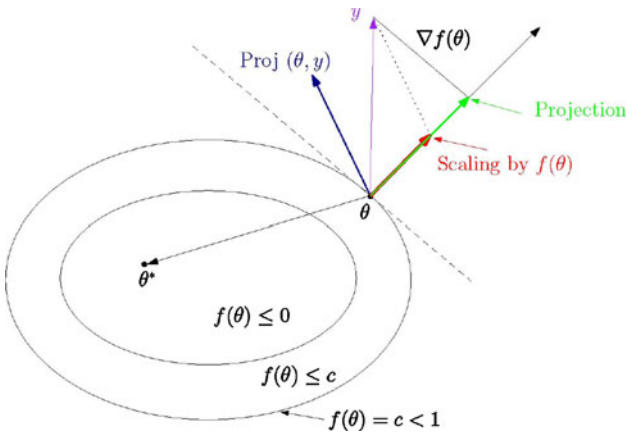

Fig. 5 Another illustration of the projection operator

of the parameter $\boldsymbol{\theta}$, belongs to Ω_0. The projection operator is defined as follows:

$$[\text{Proj}(\boldsymbol{\theta}, \boldsymbol{y}) : = \begin{cases} \boldsymbol{y} & \text{if } f(\boldsymbol{\theta}) < 0, \\ \boldsymbol{y} & \text{if } f(\boldsymbol{\theta}) \geq 0 \text{ and } \nabla f^\top \boldsymbol{y} \leq 0, \\ \boldsymbol{y} - \underbrace{\frac{\nabla f}{\|\nabla f\|}}_{\text{unit vector}} \underbrace{\langle \frac{\nabla f}{\|\nabla f\|}, \boldsymbol{y} \rangle}_{\text{projection}} \underbrace{f(\boldsymbol{\theta})}_{\text{scaling}} & \text{if } f(\boldsymbol{\theta}) \geq 0 \text{ and } \nabla f^\top \boldsymbol{y} > 0. \end{cases}$$

A projection operator has the following properties.

- For every $\boldsymbol{y}$ and $\boldsymbol{\theta}$, $(\boldsymbol{\theta} - \boldsymbol{\theta}^*)^\top (\text{Proj}(\boldsymbol{\theta}, \boldsymbol{y}) - \boldsymbol{y}) \leq 0$ since

$$(\boldsymbol{\theta} - \boldsymbol{\theta}^*)^\top (\text{Proj}(\boldsymbol{\theta}, \boldsymbol{y}) - \boldsymbol{y}) \in \left\{ 0, \left(\underbrace{(\boldsymbol{\theta}^* - \boldsymbol{\theta})^\top \nabla f}_{\leq 0} \underbrace{\nabla f^\top \boldsymbol{y}}_{> 0} \underbrace{f(\boldsymbol{\theta})}_{\geq 0} \right) \right\}.$$

- For $\boldsymbol{\theta} \in \{\boldsymbol{\theta} \in \mathbb{R}^n | f(\boldsymbol{\theta}) \leq 0\}$, $\text{Proj}(\boldsymbol{\theta}, \boldsymbol{y})$ does not alter $\boldsymbol{y}$.
- For $\boldsymbol{\theta} \in \{\boldsymbol{\theta} \in \mathbb{R}^n | 0 \leq f(\boldsymbol{\theta}) \leq 1\}$, $\text{Proj}(\boldsymbol{\theta}, \boldsymbol{y})$ subtracts a vector normal to the boundary of $\{\boldsymbol{\theta} \in \mathbb{R}^n | f(\boldsymbol{\theta}) = c\}$. The result is a smooth transformation from the original vector field $\boldsymbol{y}$ to a tangent vector field at $f(\boldsymbol{\theta}) = 1$.

$\mathcal{L}_1$ Adaptive controller for nonlinear strict feedback systems with unmodelled dynamics

Let us consider the following system:

$$\begin{aligned} \dot{x}_1(t) &= f_1(x_1(t), z(t), t) + x_2(t), \\ \dot{x}_2(t) &= f_2(x(t), z(t), t) + \mu(t), \quad \mu(s) = F(s)u(s), \\ z(t) &= g_0(x_z(t), t), \quad \dot{x}_z = g(x_z(t), x(t), t), \end{aligned}$$

where $x(t) = [x_1(t) \quad x_2(t)]^\top$ is the measured state vector, $x(0) \triangleq x_0 = [x_{1_0} \quad x_{2_0}]^\top$, and $u(t) \in \mathbb{R}$ is the control signal, $F(s)$ is an unknown stable proper transfer function that represents the uncertainties due to unmodelled dynamics, $z(t)$ and $x_z(t)$ are the output and the state vector of the unmodelled dynamics. Let $X_1(t) = [x_1(t) \quad z^\top]^\top$ and

$X(t) = [x^\top(t) \quad z^\top]^\top$. Also, let the nonlinear functions f_1, f_2, g_0 and g satisfy the following assumptions:

1. For any $\delta > 0$, there exist $K_\delta > 0$ and $B > 0$ such that $|f_1(0,u,t)| \le B$, $|f_2(0,u,t)| \le B$, $|f_1(X,u,t) - f(\bar{X},u,t)| \le K_{1_\delta}\|X - \bar{X}\|_\infty$, $|f_2(X_1,u,t) - f_2(\bar{X}_1,u,t)| \le K_{2_\delta}|X_1 - \bar{X}_1|$, and $\|X\|_\infty \le \delta$, $\|\bar{X}\|_\infty \le \delta$ uniformly in u and t.
2. The z-dynamics are bounded-input-bounded-output (BIBO) stable, i.e., there exist $L_1 > 0$ and $L_2 > 0$ such that $\|z_t\|_{\mathcal{L}_\infty} \le L_1\|x_t\|_{\mathcal{L}_\infty} + L_2$.
3. There exist upper and lower bounds $\omega_u > \omega_l > 0$ such that $\omega_l \le \frac{\partial f(x,u,t)}{\partial u} \le \omega_u$.
4. For any $\delta > 0$, there exist $d_{f_x}(\delta) > 0$, and $d_{f_t}(\delta) > 0$ such that for any u and $\|X\|_\infty < \delta$, the partial derivatives of $f(X, u, t)$ with respect to x and t are piecewise continuous and bounded

$$\left\|\frac{\partial f(X,u,t)}{\partial x}\right\| \le d_{f_x}(\delta), \quad \left\|\frac{\partial f(X,u,t)}{\partial t}\right\| \le d_{f_t}(\delta).$$

5. There exists $L_F > 0$ such that $\|F(s)\|_{\mathcal{L}_1} \le L_F$.

The control objective is to design an adaptive controller $u(t)$ to ensure that $x_1(t)$ tracks the output response of a given desired system to a bounded reference input $r(t)$.

Equivalent LTV system formulation

In addition to above assumptions, if $\|x_t\|_{\mathcal{L}_\infty} \le \rho$ then there exist $\theta(\tau)$, $\sigma(\tau)$, $\omega(\tau)$ over $[0,t]$ with $|\theta(\tau)| < \theta_b$, $|\sigma(\tau)| < \sigma_b$, $\omega_l < \omega(\tau) < \omega_u$ such that the nonlinear function $f(x, z, u, t)$ can be re-written in the following equivalent LTV form $f(x,z,u,t) = \theta(t)\|x(t)\|_{\mathcal{L}_\infty} + \omega u(t) + \sigma(t)$, where z is the unmodelled dynamics, x is the system state, u is the control signal.

$\mathcal{L}_1$ Adaptive controller

We shall first introduce some notions before describing the controller architecture. Let

$$A_m = \begin{bmatrix} -a_1 & 0 \\ 0 & -a_2 \end{bmatrix},$$

with $a_1, a_2 \in \mathbb{R}^+$. Since it is a Hurwitz matrix, there exists $P = P^\top > 0$ that solves $A_m^\top P + PA_m = -Q$ for any $Q = Q^\top > 0$. The design involves a low pass filter of unit DC gain and relative degree at least 2. Let us call it $C_1(s)$. It also involves a strictly proper transfer function $D(s)$ and gain $k \in \mathbb{R}^+$ which leads to a stable transfer function

$$C_2(s) = \frac{\omega k D(s)}{1 + \omega k D(s)},$$

with unit DC gain. A method to choose the parameters is described in Cao and Hovakimyan (2006). Let

$$A_g = \begin{bmatrix} -a_1 & 1 \\ 0 & -a_2 \end{bmatrix},$$

and define $H(s) = (sI - A_g)^{-1}$, and $G(s) = H(s)(I - C(s))$, where

$$C(s) = \begin{bmatrix} C_1(s) & 0 \\ 0 & C_2(s) \end{bmatrix},$$

We now descrive the $\mathcal{L}_1$ adaptive controller. It comprises a state predictor, a parameter adaptation law, and a controller.

- *State predictor:* The state predictor is defined by the following equations.

$$\dot{\hat{x}}_1(t) = -a_1\tilde{x}_1(t) + \tilde{\theta}_1(t)\|x_{1_t}\|_{\mathcal{L}_\infty} + \hat{\sigma}_1 + x_2(t),$$
$$\dot{\hat{x}}_2(t) = -a_2\tilde{x}_2(t) + \tilde{\theta}_2(t)\|x_t\|_{\mathcal{L}_\infty} + \hat{\sigma}_2 + \hat{\omega}(t)u(t),$$
$$\hat{x}(0) = \hat{x}_0,$$

where $\tilde{x}(t) = \begin{bmatrix} \tilde{x}_1(t) \\ \tilde{x}_2(t) \end{bmatrix} = \begin{bmatrix} \hat{x}_1(t) - x_1(t) \\ \hat{x}_2(t) - x_2(t) \end{bmatrix}$ is the vector of prediction errors while $\hat{\theta}_1(t)$, $\hat{\theta}_2(t)$, $\hat{\sigma}_1(t)$, $\hat{\sigma}_2(t)$ and $\hat{\omega}(t)$ are the adaptive estimates.

- *Paramater adaption law:* Paramater estimates are obtained by using the following equations.

$$\dot{\hat{\theta}}_1(t) = \Gamma \text{ Proj } \left(\hat{\theta}_1(t), -\|x_{1_t}\|_{\mathcal{L}_\infty}\tilde{x}^\top(t)P[1\,0]^\top\right),$$
$$\hat{\theta}_1(0) = \hat{\theta}_{1_0} \tag{1}$$

$$\dot{\hat{\theta}}_2(t) = \Gamma \text{ Proj } \left(\hat{\theta}_2(t), -\|x_t\|_{\mathcal{L}_\infty}\tilde{x}^\top(t)P[0\,1]^\top\right),$$
$$\hat{\theta}_2(0) = \hat{\theta}_{2_0} \tag{2}$$

$$\dot{\hat{\sigma}}_1(t) = \Gamma \text{ Proj } \left(\hat{\sigma}_1(t), -\tilde{x}^\top(t)P[1\,0]^\top\right), \quad \hat{\sigma}_1(0) = \hat{\sigma}_{1_0} \tag{3}$$

$$\dot{\hat{\sigma}}_2(t) = \Gamma \text{ Proj } \left(\hat{\sigma}_2(t), -\tilde{x}^\top(t)P[0\,1]^\top\right), \quad \hat{\sigma}_2(0) = \hat{\sigma}_{2_0} \tag{4}$$

$$\dot{\hat{\omega}}(t) = \Gamma \text{ Proj } \left(\hat{\omega}(t), -u(t)\tilde{x}^\top(t)P[0\,1]^\top\right), \quad \hat{\omega}(0) = \hat{\omega}_0, \tag{5}$$

where $\Gamma \in \mathbb{R}^+$ is the adaptation gain and $Proj(\cdot,\cdot)$ is the projection operator.

- *Controller:* The control signal is given by the following equations.

$$u(s) = -k\chi(s), \quad \text{where} \quad \chi(s) = D(s)r_u(s),$$

where $r_u(s) = \mathcal{L}(r_u(t))$ and $r_u(t)$ is given by

$$r_u(t) = \hat{\omega}(t)u(t) + \hat{\eta}_2(t) + a_2(x_2(t) - \alpha(t)) - \dot{\alpha}(t),$$

with $\hat{\eta}_2(t) = \hat{\theta}_2(t)\|x(t)\|_\infty + \hat{\sigma}(t)$ and $\alpha(t) = -a_1\,(x_1(t) - r(t)) + \hat{\eta}_{1C}(t) + \dot{r}(t)$, $\hat{\eta}_{1C}(t) = \mathcal{L}^{-1}(C_1(s)\hat{\eta}_1(s))$, $\hat{\eta}_1(t) = \hat{\theta}_1(t)|x_1(t)| + \hat{\sigma}_1(t)$.

Synthesis of the $\mathcal{L}_1$ adaptive controller for the MAPK cascade

Since the MAPK cascade is subject to exogenous disturbances, the kinetic constants are not precisely known and are liable to change. We therefore use an $\mathcal{L}_1$ adaptive controller to synthesize the oscillations. Our approach is as follows:

- Design a baseline controller for a nominal system model and tune the gains to ensure oscillations of desired amplitude and frequency.
- Design an $\mathcal{L}_1$ (augmentation) controller for the system defined by the error between the actual system and the reference system, where both these systems have closed loops with a nominal integral controller.

The following control structure is employed for the nominal system:

$$\dot{k}_{in} = \omega_1(M - 250) + \frac{\omega_2}{k_{in} + 1}$$

This controller is an integrator which is often used to induce oscillations in a system that exhibits a hysteretic steady state structure; a well-known example is the Van der Pol oscillator (see Stan 2005). The results of a bifurcation analysis with $\omega_2 = 1$ are described in Fig. 6 and show a narrow band of high amplitude desirable oscillations. These are observed around $\omega_1 \approx 0.001$. Figure 6 is a bifurcation diagram describing the steady-state values of M_{pp} as a function of the gain ω_1 while ω_2 is held fixed at the value equal to 1. The bifurcation diagram was drawn using the numerical continuation software AUTO2000 (Doedel et al. 2000). For very small values of ω_1, the dynamics possess a stable equilibrium solution. Around

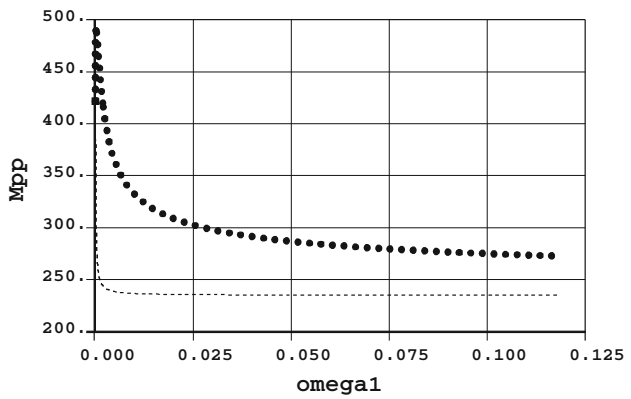

Fig. 6 Plot of the steady-state values of M_{pp} as a function of ω_1. The *circles* denote the amplitude of the stable limit cycle whereas the dashed line denotes unstable equilbria. The *square* denotes a Hopf bifurcation. This plot is obtained for $\omega_2 = 1$. It may be noted that oscillations of the desired amplitude are obtained for a narrow range of values of ω_1 around the Hopf bifurcation point

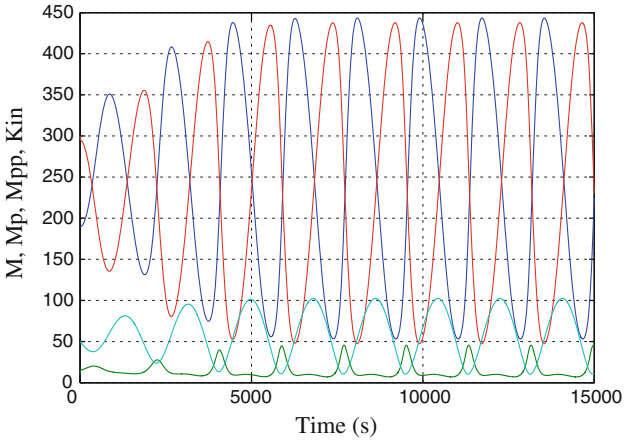

Fig. 7 Oscillations in M, M_p, M_{pp}, and K_{in} for the case of $\omega_1 = 0.0008$ and $\omega_2 = 1$

$\omega_1 = 0.0002$, the equilibrium becomes unstable via a supercritical Hopf bifurcation (denoted by a square in Fig. 6) to give rise to stable limit cycles. The amplitude of the limit cycles (denoted by circles) initially increases rapidly before settling down to values between 250 and 300. The amplitude of the oscillations is desirably large for a very narrow range of ω_1 around the Hopf bifurcation. In this narrow band, as seen in Fig. 7, the oscillations exhibit a relaxation oscillator-like behaviour. Indeed, as noted earlier, the closed loop dynamics resemble those of a Van der Pol oscillator with one important difference: the amplitude of the limit cycles of a Van der Pol oscillator is constant for all values of the integrator gain, i.e., ω_1 (see Strogatz 1994). It is interesting to note that several biological systems are known to demonstrate persistent oscillations in the close vicinity of Hopf bifurcations, and our system is no exception.

Simulation results with $\omega_1 \approx 0.0008$ are shown in Fig. 7. Figure 8 shows the plot of Hopf bifurcation in $\omega_1 - \omega_2$

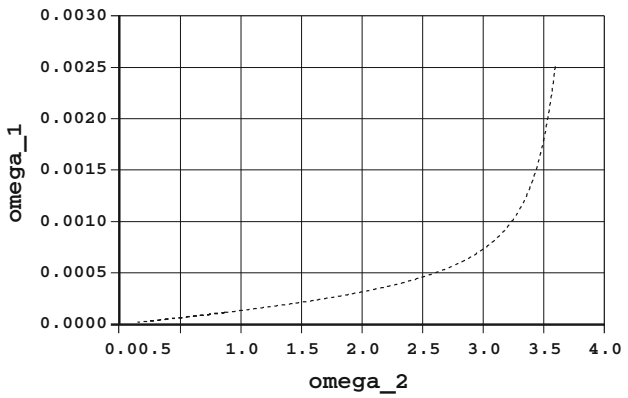

Fig. 8 The locus of Hopf bifurcations in the $\omega_1 - \omega_2$ parameter space. As in Fig. 6, we observe that the high amplitude oscillations in M and M_{pp} are obtained for parameter values close that are quite close to the Hopf bifurcation point

parameter space. The control design process involves the selection of gains ω_1 and ω_2. Our synthesized controller is an integrator with a nonlinearity which becomes stronger as ω_2 is increased. The nonlinearity prevents k_{in} from decreasing below zero, and the value of ω_2 is chosen accordingly. Once ω_2 is chosen, ω_1 needs to be chosen to ensure that the oscillations possess the desired amplitude. The corresponding value of ω_1, as noted earlier, is close to the Hopf bifurcation. The locus of the Hopf bifurcation in the ω_1-ω_2 parameter space canbe obtained to aid the selection of ω_1. Figure 8 is drawn usingthe numerical continuation software AUTO2000 (Doedel et al. 2000).It turns out that in order to get high amplitude oscillations at lower frequency—these oscillations are close to the Hopf bifurcation—we need to reduce the value of ω_2. This shows that the value of ω_1 needs to be well-tuned given ω_2. Since the kinetic constants in the MAPK cascade are not known precisely,we shall use a $\mathcal{L}_1$ adaptive controller to solve this problem as follows.

1. We shall first derive equations for the error dynamics of the actual system with respect to the nominal system.
2. We shall then derive equations for the error in M and u, and shall treat the error in M_{pp} as a time-varying disturbance for the purpose of regulation.
3. The system is now in a strict feedback form for which we use the controller derived in Paranjape et al. (2009).

The block diagram of the control system is shown in Fig. 9a, b. The controller block consists of all components of the $\mathcal{L}_1$ control system—the control signal generator, the

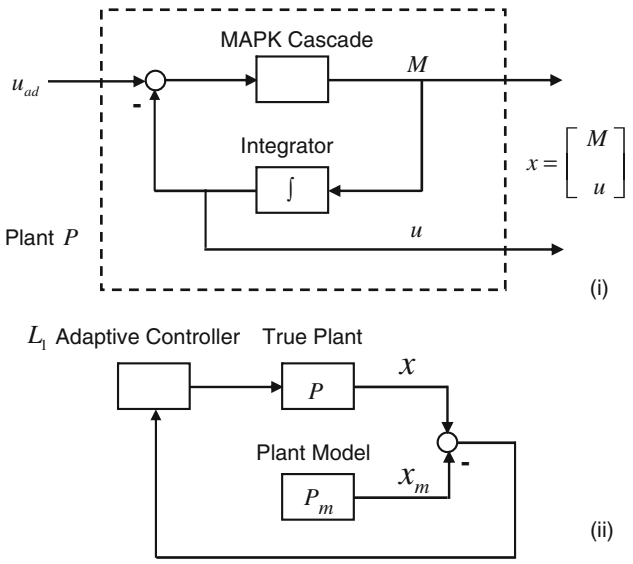

Fig. 9 **a** Structure of the plant P. **b** Block diagram of the $\mathcal{L}_1$ adaptive control system

predictor and the low pass filter. The actual system $\mathcal{S}_1$ can be written as

$$\dot{x} = f(x,\mu) + g(x,\mu)u, \quad \dot{u} = kx_1 + h(u) + u_{ad}$$

where $x = \left[M,\ M_{pp}\right]^\top$, u represents the integral control, and u_{ad} is the adaptive augmentation added to the system. The nominal system is now re-cast as

$$\dot{x_n} = f(x_n,\mu_n) + g(x,\mu)u, \quad \dot{u} = kx_{n_1} + h(u_n).$$

Note that the difference in the actual system and the nominal system is due to the difference in the parameter values and due to the time-varying disturbance.

Let $e_1 = M - M_n$ and $e_2 = u - u_n$. Using the equivalent LTV system formulation explained in Cao and Hovakimyan (2008), the dynamics may be written as

$$\dot{e}_1(t) = \theta_1(t)\|e_{x_t}\|_{\mathcal{L}_\infty} + \sigma_1(t) + \omega(t)e_2(t)$$
$$\dot{e}_2(t) = \theta_2(t)\|e_{x_t}\|_{\mathcal{L}_\infty} + \sigma_2(t) + u_{ad}(t)$$

where $e_x = \left[M - M_n\ M_{pp} - M_{pp,n}\right]^\top$ and $e_u = [M - M_n\ M_{pp} - M_{pp,n}\ u - u_n]^\top$. Further, for a variable z, $\|z\|_{\mathcal{L}_\infty}$ denotes its truncated $\mathcal{L}_\infty$ norm. The state predictor is given by

$$\dot{\hat{e}}_1(t) = -a_1\tilde{e}_1(t) + \hat{\theta}_1(t)\|e_{x_t}\|_{\mathcal{L}_\infty} + \hat{\sigma}_1(t) + \hat{\omega}(t)e_2(t)$$
$$\dot{\hat{e}}_2(t) = -a_1\tilde{e}_2(t) + \hat{\theta}_2(t)\|e_{x_t}\|_{\mathcal{L}_\infty} + \hat{\sigma}_2(t) + u_{ad}(t)$$

Here, $a - 1$, $a_2 > 0$, $\tilde{e}_i = \hat{e}_i - e_i$ for $i = 1, 2$. If we let $A = \begin{bmatrix} -a_1 & 0 \\ 0 & -a_2 \end{bmatrix}$, then we note that A is Hurwitz and hence for any $Q = Q^\top > 0 (Q \in \mathbb{R}^{2\times 2})$, there exists $P = P^\top > 0$ which solves the Lyapunov equation $A^\top P + PA = -Q$. Let $e \doteq [e_1\ e_2]^T$. The projection-based adaptation laws are given by the Eqs. (1)–(5). Finally, let $\alpha(s) = -kD(s)(a_1e_1(s) + \hat{r}_1(s))$, where $\hat{r}_1(s)$ is the Laplace transformation of $\hat{r}_1(t) = \theta_1(t)\|e_{x_t}\|_{\mathcal{L}_\infty} + \sigma_1(t) + \omega(t)e_2(t)$. The control signal is defined via the following feedback loop:

$$u(s) = -a_2(e_2(s) - \alpha(s)) - C_2(s)\hat{r}_2(s) + \mathcal{L}(\dot{\alpha}(t))$$

where $\hat{r}_2(t) = \hat{\theta}_2(t)\|e_{u_t}\|_{\mathcal{L}_\infty} + \hat{\sigma}_2(t)$. The constant $k > 0$, and the filters $D(s)$ and $C_2(s)$ have to be tuned to satisfy the $\mathcal{L}_1$ norm condition state below. The filter $D(s)$ should have at least one integrator. Let $\omega > 0$ be a constant and denote the mean value of $\omega(t)$, which is positive, and let $C_1(s) = \frac{\omega kD(s)}{1+\omega kD(s)}$. One should choose k and $D(s)$ so that $C_1(s)$ has a relative degree of at least 2, while $C_2(s)$ should have a relative degree of at least 1.

We next state the $\mathcal{L}_1$ norm condition. For $\rho > 0$, let L_ρ be the known estimate for the Lipzchitz constant of the unknown nonlinearities. This is the finite bound on $\theta_i(t)$ for $i = 1,2$. Let $B > 0$ be the uniform bound on the $\sigma_i(t)$ for

$i = 1,2$. Let the transfer function matrix $H(s)$ be given by $H(s) = (s\mathbb{I} - A_g)^{-1} = \begin{bmatrix} \frac{1}{s+a_1} & \frac{1}{(s+a_1)(s+a_2)} \\ 0 & \frac{1}{s+a_2} \end{bmatrix}$, where $A_g = \begin{bmatrix} -a_1 & 1 \\ 0 & -a_2 \end{bmatrix}$. Let $G(s) = H(s)(\mathbb{I} - C(s))$, where $C(s) = \begin{bmatrix} C_1(s) & 0 \\ 0 & C_2(s) \end{bmatrix}$. To ensure that the system stable and that the performance bounds are met, the selection of $C_1(s)$, k and $D(s)$ must ensure that there exists $\rho_r(s) > 0$ such that:

$$\|G(s)\|_{\mathcal{L}_1} < \frac{\rho_r - \xi}{L\rho_r + \zeta}$$

where $L = (1 + a_1 + \|C_1(s)\|_{\mathcal{L}_1} L_\rho)((a_1 + 1 + a_2\|C_1(s)\|_{\mathcal{L}_1} + \|sC_1(s)\|_{\mathcal{L}_1})L_\rho + a_2(a_1 + 1) + a_1)$, $\zeta = (1 + a_1 + \|C_1(s)|_{\mathcal{L}_1} L_\rho)((a_1 + 1 + a_2\|C_1(s)\|_{\mathcal{L}_1} + \|sC_1(s)\|_{\mathcal{L}_1})B)$, $\xi = (1 + a_1 + \|C_1(s)\|_{\mathcal{L}_1} L_\rho)\|e_m\|_{\mathcal{L}_\infty} + \|C_1(s)\|_{\mathcal{L}_1} B$, $e_m(s) = H(s)e_0$. Finally, $\rho = \rho_r + \gamma$ for an arbitrary constant $\gamma > 0$.

Remark 5 The adaptation rate should be chosen to ensures that the error between system and predictoris bounded from above by γ. The $\mathcal{L}_1$ condition used by us may facilitate a conservative filter design. It is best to tune the filters manually. For example, using the above condition can yield higher filter bandwidths whereas much lower bandwidths may suffice in practice.

Simulation results

We simulate our controller. The actual system parameters are displaced from those of the nominal system. For the nominalsystem, we choose $\omega_1 = 0.0004$ and $\omega_2 = 0.1$, which generates oscillations similar to the one in Fig. 7, albeit at a reduced frequency. We choose the following control design for the adaptive augmentation controller: $a_1 = a_2 = 0.5$, $k = -20$, $D(s) = \frac{1}{s^2+10s}$, $C_2(s) = \frac{16}{s^2+80s+16}$.

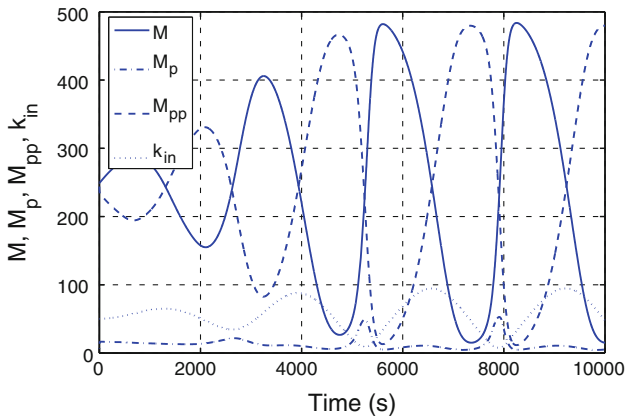

Fig. 10 M, M_p, M_{pp}, u for the actual as well as nominal system

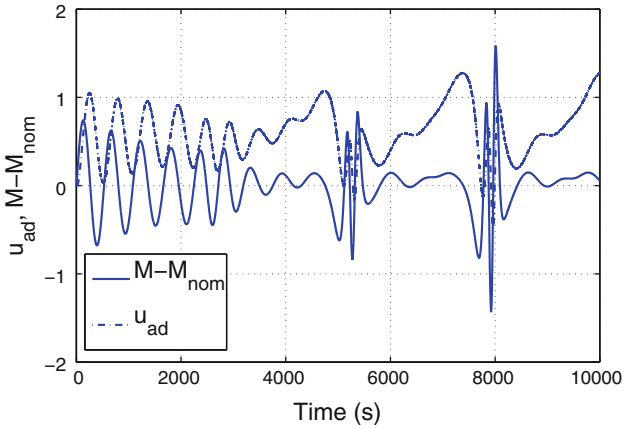

Fig. 11 (i) Evolution of the error $M - M_n$ as a function of time. (ii) Evolution of the adaptive augmentation signal $u_{ad}(t)$ as a function of time

As Fig. 10 shows, the values of M, M_p, M_{pp}, u for the actual system match satisfactorily with those for the nominal system (Fig. 10). It is seen that they match satisfactorily. The error between M and M_n is shown in Fig. 11a and the adaptive augmentation signal is shown in Fig. 11b. It is seen that the error goes down rapidly, while after about 1000 seconds, the adaptive augmentation control becomes periodic. This is because the actual system is displaced from the nominal system in its parameters, and because all signals are periodic, a periodic augmentation is needed to ensure that the actual and nominal system track each other. We have chosen the adaptive gain as $\Gamma = 10,000$, but it can be increased without any loss of robustness or high frequency noises. This controller is robust to external disturbances, internal parameter variations as well as unmodelled dynamics as long as they are stable—mathematical proofs for the generic case of nonlinear strict feedback systems are derived in Paranjape et al. (2009).

Discussion

MAPK Fus3 is a key regulator of the yeast mating pheromone response and is known to undergo sustained oscillations in its phosphorylation/activation state during continuous pheromone exposure (see Hilioti et al. 2008). The MAPK activity oscillations lead to corresponding oscillations in the mating gene expression. These oscillations in MAPK activity and gene expression have been empirically observed to need the negative regulator of G-protein signaling Sst2, and partially need the MAPK phosphatase Msg5. The peaks in Fus3 activation are correlated with periodic rounds of cell morphogenesis, with each peak preceding the formation of an additional mating projection (see Hilioti et al. 2008). Fus3-GFP and

Fus1-GFP protein levels display strong oscillatory dynamics with frequencies similar to the oscillations of Fus3 activation. Furthermore, increasing the pheromone dose has been observed to result in a progressive phase shift of Fus3-GFP expression peaks towards earlier time points; this trend is also observed for phospho-MAPK levels so that it is now established that the expression levels of MAPK target genes oscillate in approximate synchrony with MAPK activation levels (see Hilioti et al. 2008). Likewise, the effect of MAPK cascade oscillations on the hippocampal neuron memory has recently been characterized (see Gerstner et al. 2009). So, an elaborate control over some cellular functions may be exercised by controlling oscillations in the MAPK cascade.

We have used the bifurcation analysis to determine the parameter values required to obtain the desired oscillations. In addition, we have used the bifurcation analysis to determine the sensitivity of the amplitude of oscillations to the parameters. Large amplitude oscillations are obtained only in the close vicinity of the Hopf bifurcation. Indeed, several systems found in the human body, such as the oculomotors and hair cells in the cochlea, operate very close to Hopf bifurcations (Moreau and Sontag 2003). Operating close to the bifurcation point ensures that large amplitude oscillations encounter minimal damping and are hence sustained.

Our $\mathcal{L}_1$ adaptive controller synthesis approach can be used to synthesize feedback that induces tunable robust oscillations of desired frequency in a network of MAPK cascades as well. Our approach quantifies the transient and steady-state performance bounds of the $\mathcal{L}_1$ adaptive backstepping controller in the presence of fast adaptation. These bounds can be systematically increased by increasing the adaptation rate. $\mathcal{L}_1$ adaptive control architecture guarantees robustness in the presence of fast adaptation. The robustness to parameter variations and disturbances is ensured by suitably modifying the control objective with the understanding that the uncertainties can be adequately compensated for only if the controller bandwidth is high enough—the constraints imposed by robustness requirements on the limits of achievable performance in closed-loop systems are well illustrated in Chaps. 3 and 6 (Skogestad and Postlethwaite 2005). With the $\mathcal{L}_1$ adaptive control architecture, it appears that a fast rate of adaptation helps meet the performance specifications and also ensures the required robustness margins—the trade-off between these two requirements is to be resolved using the filter (see Li et al. 2008).

An advantage of our $\mathcal{L}_1$-control theory approach is that it enables us to decouple the problem of meeting the performance specifications and the problem of ensuring robustness to parameter variations and disturbances: the performance can be improved systematically by increasing the adaptation gain whereas the robustness is guaranteed—so long as it is feasible—by choosing an appropriate filter. Better performance than the one reported in this paper may be obtained by using a much larger adaptation gain. Unlike the traditional adaptive control methodologies, the maximum adaptation gain is restricted only by limitations of the components used to implement the $\mathcal{L}_1$ controller. In traditional control theoretic applications (e.g., aircraft altitude control and automotive engine speed control), these limitations refer to the hardware limitations whereas in a systems and synthetic biology setting, these refer to the quality of the scaffold and the speed of the chemical reactions—these implementation aspects are well discussed in Kharam et al. (2011) and Jiang et al. (2010).

Conclusion

MAPK cascade is evolutionally preserved in all eukaryotic cells, and regulates various cellular activities such as gene expression, mitosis, differentiation, and apoptosis. Recently, in Bashor et al. (2008), have shown that Ste5 scaffold protein can be used to reshape the MAPK cascade through engineered feedback loops, and have used heuristic tuning mechanisms to synthesize the feedback . A problem of interest is to determine whether information regarding the underlying biochemical reactions can be used to synthesize robust feedback that will ensure that the resultant circuit has the desired properties. In this paper, we have examined the problem of engineering feedback in MAPK cascade to synthesize an oscillator of the desired frequency. Our approach builds on the MAPK cascade model derived by Chikarmane et al. in 2007. In Chikarmane et al. (2007), the existence of a Hopf bifurcation point in the Markevich model of the MAPK cascade is used to synthesize the exciting kinase as a function of the doubly phosphorylated protein. We show how the $\mathcal{L}_1$-control theory can be used for a robust synthesis of the desired oscillator. Our $\mathcal{L}_1$ controller is robust to changes in the kinetic parameters of the MAPK cascade. The resultant oscillations are provably stable. Furthermore, it can be shown that the error in the desired states and the actual states asymptotically approaches zero and is upper bounded during the transient response phase.

References

Bashor C, Helman N, Yan S, Lim W (2008) Using engineered scaffold interactions to reshape MAP kinase pathway signaling dynamics. Sci Agric 319(14):1539–1543

Cao C, Hovakimyan N (2006a) Design and analysis of a novel $\mathcal{L}_1$ adaptive controller, part I: control signal and asymptotic stability. In: Proceedings of the 2006 American control conference. Minneapolis, Minnesota, pp 3397–3402

Cao C, Hovakimyan N (2006b) Design and analysis of a novel $\mathcal{L}_1$ adaptive controller, part II: guaranteed transient performance. In:

Proceedings of the 2006 American control conference. Minneapolis, Minnesota, pp 3403–3408

Cao C, Hovakimyan N (2008) $\mathcal{L}_1$ adaptive controller for a class of systems with unknown nonlinearities: part 1. In: Proceedings of the American control conference, pp 4093–4098

Chikarmane V, Kholodenko B, Sauro H (2007) Oscillatory dynamics arising from competitive inhibition and multisite phosphorylation. J Theor Biol 244:68–76

Doedel E, Paffenroth R, Champneys A, Fairgrieve T, Kuznetsov Y, Oldeman B, Sandstede B, Wang X (2000) Auto2000: Software for continuation and bifurcation problems in ordinary differential equations. Technical report, California Institute of Technology, Pasadena

Georgiou T, Smith M (2000) Robustness of relaxation oscillators. In: The proceedings of the conference on decision and control, Sydney, Australia, pp 246–250

Gerstner JR, Lyons LC Jr, KPW, Loh DH, Rawashdeh O, Eckel-Mahan KL, Roman GW (2009) Cycling behavior and memory formation. J Neurosci 29(41):12824–12830

Hasty J, Dolnik M, Rottschafer V, Collins J (2001) Synthetic gene network for entraining and amplifying oscillations. Phys Rev Lett 88(14):148101–148104

Hilioti Z, W. Sabbagh J, Paliwal S, Bergmann A, Goncalves M, Bardwell L, Levchenko A (2008) Oscillatory phosphorylation of yeast Fus3 MAP kinase controls periodic gene expression and morphogenesis. Curr Biol 18(21):1700–1706

Huang C, Ferrell J (1996) Ultrasensitivity in the mitogen-activated protein kinase cascade. PNAS 93:10078–10083

Ioannou P, Sun J (1996) Robust adaptive control. Prentice Hall, Englewood Cliffs

Jiang H, Kharam A, Riedel M, Parhi K (2010) A synthesis flow for digital signal processing with biomolecular reactions. In: International conference on computer aided design. San Jose, CA

Khalil HK (2002) Nonlinear systems, 3rd edn. Prentice Hall, Englewood Cliffs

Kharam A, Jiang H, Riedel M, Parhi K (2011) Filter design for feedback loop trade-off of $\mathcal{L}_1$ adaptive control: a linear matrix inequality approach. In: Pacific symposium on biocomputing. Honolulu, HI

Kholodenko B, Kiyatkin A, Bruggeman F, Sontag E, Westerhoff H, Hoek J (2002) Untangling the wires: a strategy to trace functional interactions in signaling and gene networks. PNAS 99(20):12841–12846

Li D, Hovakimyan N, Cao C, Wise K (2008) Filter design for feedback loop trade-off of $\mathcal{L}_1$ adaptive control: a linear matrix inequality approach. In: Proceedings of the AIAA guidance, navigation and control conference. Honolulu, HI

Markevich N, Hoek J, Kholodenko B (2004) Signaling switches and bistability arising from multisite phosphorylation in protein kinase cascades. J Cell Biol 164:353–359

Moreau L, Sontag E (2003) Balancing at the border of instability. Phys Rev E Stat Nonlinear Soft Matter Phys 68(2):020901–020904

Paranjape A, Xargay E, Hovakimyan N, Cao C (2009) Guaranteed transient performance with $\mathcal{L}_1$ adaptive controller for nonlinear strict feedback systems. Mediterranean conference on control and automation, pp 229–234. doi:10.1109/MED.2009.5164544

Qiao L, Nachbar R, Kavrekidis I, Shvartsman S (2007) Bistability and oscillations in the Huang-Ferrell model of MAPK signalling. PLoS Comput Biol 3(9):1819–1826

Skogestad S, Postlethwaite I (2005) Multivariable feedback control: analysis and design, 2nd edn. Wiley, Chichester

Stan GB (2005) Global analysis and synthesis of oscillations: a dissipativity approach. Ph.D. thesis, Université De Liège

Stan GB, Sepulchre R (2007) Analysis of interconnected oscillators by dissipativity theory. IEEE Trans Automat Control 52(2):256–270

Strogatz S (1994) Nonlinear dynamics and chaos with applications to physics, biology, chemistry and engineering. Westview Press, Boulder

Varigonda S, Georgiou T (2001) Dynamics of relay relaxation oscillators. IEEE Trans Automat Control 46(1):65–77

Wang X, Hao N, Dohlman H, Elston T (2006) Computational and experimental analysis of bistability, stochasticity, and oscillations in the mitogen activated protein kinase cascade. Biophys J 90:1961–1978

Zheng B, Fiumara P, Li Y, Georgakis G, Snell V, Younes M, Vauthey J, Carbone A, Younes A (2003) MEK/ERK pathway is aberrantly active in hodgkin disease: a signaling pathway shared by cd30, cd40, and rank that regulates cell proliferation and survival. Blood 102(3):1019–1027